

Considering Photoinduced Second-Harmonic Generation as a dc Kerr Optical Parametric Oscillation or Amplification Process

Xiyuan Lu^{1,2,*} and Kartik Srinivasan^{1,3,†}

¹ Microsystems and Nanotechnology Division, Physical Measurement Laboratory, National Institute of Standards and Technology, Gaithersburg, Maryland 20899, USA

² Institute for Research in Electronics and Applied Physics and Maryland NanoCenter, University of Maryland, College Park, Maryland 20742, USA

³ Joint Quantum Institute, NIST/University of Maryland, College Park, Maryland 20742, USA



(Received 20 December 2020; revised 3 June 2021; accepted 10 June 2021; published 12 July 2021)

Photoinduced second-harmonic generation (SHG) in centrosymmetric materials like silica and silicon nitride has been commonly explained as an effective second-order ($\chi^{(2)}$) process mediated by a dc electric field and the medium's third-order ($\chi^{(3)}$) nonlinearity. In this explanation, the coherent photogalvanic effect is the source of a dc electric field whose spatial periodicity naturally enables quasi-phase-matching. While successful in explaining many observations from experiment, the behavior at low input powers, and in particular, the apparent existence of a threshold for efficient photoinduced SHG observed in some experiments has largely been overlooked theoretically. In this Paper, we reconsider photoinduced SHG within the framework of four-wave mixing (FWM), involving degenerate pump, second-harmonic signal, and dc electric field. We propose a hypothesis that photoinduced SHG is a FWM-mediated dc Kerr optical parametric oscillation or amplification process. This hypothesis can explain the threshold behavior, and moreover, predicts unconventional light amplification, both of which we verify by experiments in silicon-nitride microresonators. Finally, we discuss the physical implications of our work in various platforms and future directions.

DOI: 10.1103/PhysRevApplied.16.014027

I. INTRODUCTION

Photoinduced second-harmonic generation (SHG) was discovered in germanium-doped optical fiber, where intense laser light, above a threshold power of 5 kW, was found to generate second-harmonic light and amplify it over hours, resulting in high conversion efficiency up to 5% [1,2]. Given the lack of a bulk second-order ($\chi^{(2)}$) response in these fibers, the origin of such an efficient process was not initially understood and led to a burst of over 200 publications within the following decade [3]. Through these collective efforts [1–16] (Fig. 1), photoinduced SHG was largely understood on the basis of three physical effects [3]: (1) field-induced SHG (FISH) [17], where a dc electric field, together with the medium's third-order ($\chi^{(3)}$) nonlinear response, produces an effective $\chi^{(2)}$ response; (2) the coherent photogalvanic effect (CPG) [11,12], in which photodriven charge separation produces the requisite dc electric field; and (3) quasi-phase-matching (QPM) [18,19], in which a spatial periodicity in a medium's nonlinear response (in this case, the dc electric field)

compensates for wave-vector mismatch between the fundamental and second-harmonic fields.

In recent years, significant progress has been made to improve the power efficiency of photoinduced SHG using nanophotonic waveguides [20–25]. The threshold power, initially at the kW level in optical fiber [2,6,10,12], was reduced by over 100× to a few tens of watts in nanophotonic waveguides in several works [20,21,24]. Recently, we have demonstrated photoinduced SHG in a Si₃N₄ microring resonator [26], which resulted in a further reduction by over 1000× to the milliwatt level. While the composite model for photoinduced SHG is consistent with many observations from such experiments over the years, one critical omission is its inability to explain the apparent threshold behavior observed in several experiments [2,20,26]. Empirical fits have been reported [2,20], but the key physical understanding of why such a threshold exists in a SHG process (which in conventional situations is thresholdless) and how to estimate the threshold power have been overlooked for decades. Appendix A provides further details on the history and background of photoinduced SHG. Interestingly, the reduction of threshold power from kilowatt level in optical fibers, to watt level in nanophotonic waveguides and milliwatt level in

*xiyuan.lu@nist.gov

†kartik.srinivasan@nist.gov

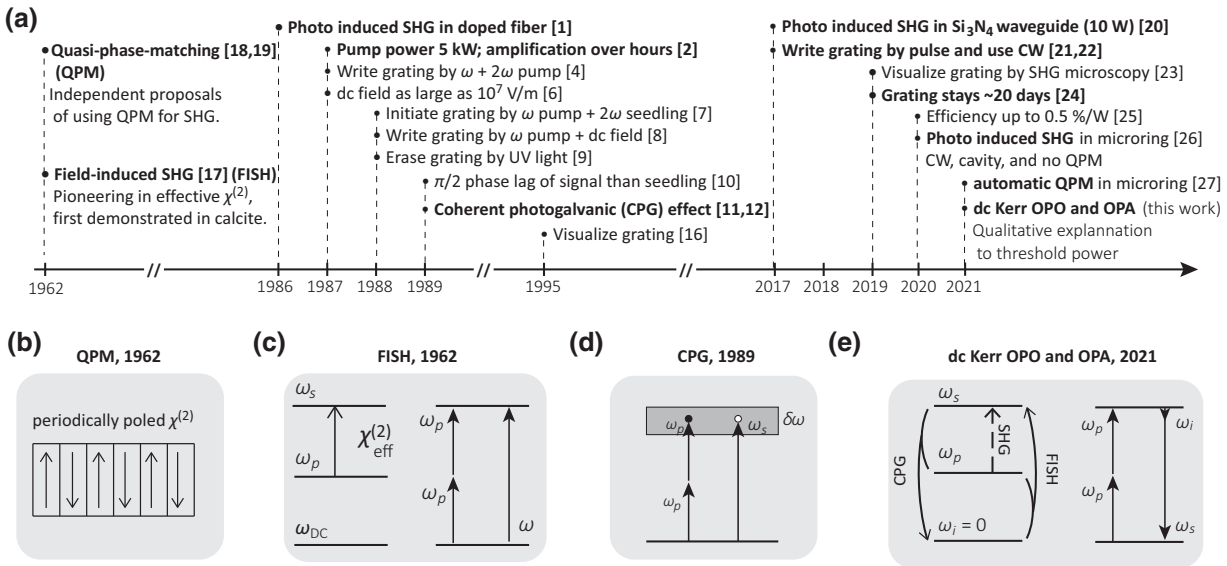


FIG. 1. History and physical mechanisms behind photoinduced SHG. (a) Timeline of photoinduced SHG, where dots are aligned to the year when events were reported. Photoinduced SHG was discovered in 1986 in doped fiber and subsequently extensively studied in the next decade, through the incorporation of three related theoretical models: (b) quasi-phase-matching (QPM), (c) field-induced SHG (FISH), and (d) the coherent photogalvanic effect (CPG). Various schemes have been explored, mostly in doped optical fibers, in writing, initiating, and erasing the photoinduced grating for QPM and the dc electric field that enables phase and frequency matching of the SHG process based on an effective $\chi^{(2)}$ framework. Photoinduced SHG has seen a revival of interest in recent years, in particular, in Si₃N₄ waveguides and microrings. (e) In this work, we study photoinduced SHG in a Si₃N₄ microring, where efficiency is high, QPM is not required, and a continuous-wave pump is used. We show that photoinduced SHG can be considered as a dc Kerr optical parametric oscillation and amplification process, from which a threshold behavior is naturally expected, and which matches well with experimental results.

microrings, closely resembles the reduction of threshold powers of optical parametric oscillator (OPO) devices based on parametric nonlinear-wave-mixing processes (see Appendix E for details).

To this end, the microring platform [26,27] is ideal for studying the threshold behavior. In the microring, photoinduced SHG is achieved through the interaction of three cavity modes, namely, two optical modes (fundamental and second harmonic) and a dc electric field. In our platform particularly [26], SHG is achieved under continuous-wave conditions with the modes being perfectly phase matched, and the characteristic timescale of the process is in the range of seconds to a couple of minutes (much faster than in previous works [24,27]). These features make a study of the threshold for photoinduced SHG particularly simple in comparison to earlier works in Si₃N₄ waveguides [21–25], in which amplified short pulses were used, QPM was needed, and the timescale of the process ranged from hours to days.

Here, we present a theoretical model in which photoinduced SHG is considered to result from the $\chi^{(3)}$ process of dc Kerr optical parametric oscillation and amplification (OPO and OPA). This perspective naturally captures the threshold behavior, which is verified by experiment. We also show unconventional light amplification in a sum-frequency generation regime beyond conventional

$\chi^{(2)}/\chi^{(3)}$ OPO and OPA, which is consistent with our theoretical prediction. Quantitative agreement with our experimental results can be obtained if certain conditions on the dc field are satisfied, whose physical implications we outline. Our results provide an alternative perspective on the physics of photoinduced SHG, and can help open a frontier of efficient dc $\chi^{(3)}$ nonlinear optics.

II. THEORY

We study the photoinduced SHG process inside a cavity with two optical modes and a dc electric mode, as shown in Fig. 1(e). The threshold behavior in such a system has not been explained by FISH [Fig. 1(c)] and/or CPG [Fig. 1(d)] as considered in other works up to this point. Instead, if we consider both FISH and CPG as parts of a dc-field-mediated four-wave-mixing process, the threshold behavior will naturally emerge in resemblance to the conventional $\chi^{(3)}$ OPO (i.e., with all interacting fields at optical frequencies). We note that in the frequency diagram of dc degenerate four-wave mixing (dc DFWM), although $\omega_i = 0$, it is nevertheless worthwhile to explicitly show its presence. Without acknowledging its presence, this model reduces to an effective $\chi^{(2)}$ model, which appears to be thresholdless. Put in other words, the effective $\chi^{(2)}$ framework explains only the end results after

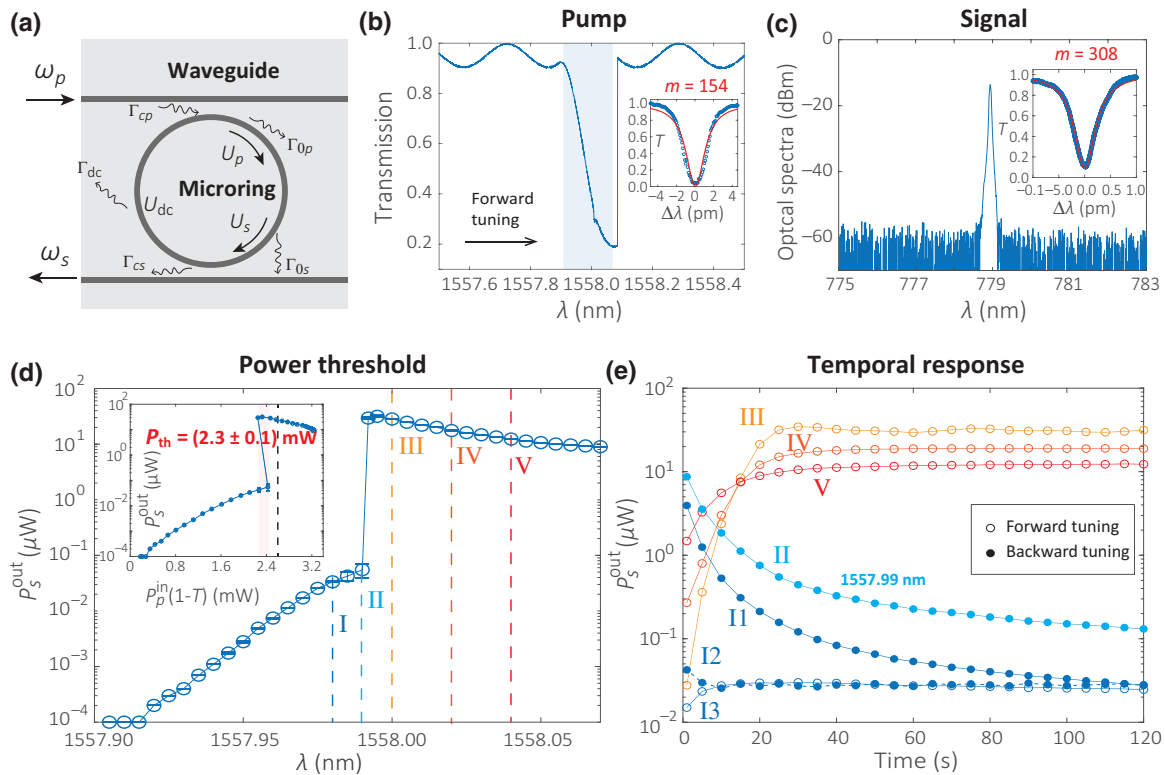


FIG. 2. dc Kerr optical parametric oscillation (OPO). (a) Schematic shows an integrated microring with coupling waveguides and related physical parameters for the pump (p), signal (s), and dc fields, in particular, intracavity energies $U_{p,s,dc}$, waveguide-resonator coupling rates $\Gamma_{cp,cs}$ and intrinsic loss rates $\Gamma_{0p,0s,dc}$. (b) Forward tuning of the pump laser shows thermal bistability. The kink (at $\lambda \approx 1558.0$ nm) is where the pump and SHG modes are frequency matched. The inset shows the cold-cavity transmission (i.e., without thermal bistability) of the pump mode with mode number of $m = 154$. (c) Optical spectrum of the second-harmonic signal at $\lambda \approx 779$ nm. The inset shows the cold-cavity transmission trace. The SHG mode has a mode number of $m = 308$. (d) Adiabatic forward tuning is used to record the threshold behavior of the SHG process. The threshold power is (2.3 ± 0.1) mW, as shown in the inset. The decrease of the power after crossing the threshold is due to the decrease of intracavity pump energy after conversion, which corresponds to an approximately 8 % intracavity conversion efficiency. The dashed lines (labeled I–V) have colors that correspond to traces in (e) with I–II below threshold, and III–V above threshold. (e) The temporal response shows distinctive properties of the dc Kerr OPO. The time constant observed in these traces agrees with a first-principles estimate of the RC time constant in silicon nitride (e.g., $\tau \approx 16$ s for trace II). Both growth and decay are observed for traces II–I3 (with different initial SHG signals), with the final power only dependent on the final laser-cavity detuning and the dropped pump power.

a nonlinear grating has been created and stabilized, but does not predict whether or when such a nonlinear grating (and amplification) can happen in the first place.

We describe photoinduced SHG in the following equations considering both $\chi^{(3)}$ and $\chi^{(2)}$ processes [Fig. 2(a)], more specifically, DFWM [28] and SHG [29], where the slowly varying envelopes of the fields are given by

$$\begin{aligned} \frac{d\tilde{A}_p}{dt} &= [i(\Delta\omega_p + \gamma_{pppp} U_p + 2\gamma_{psps} U_s) - \Gamma_{tp}/2] \tilde{A}_p \\ &\quad + 2i\gamma_{pspi}\tilde{A}_s\tilde{A}_i\tilde{A}_p^* + i\gamma_{psp}\tilde{A}_s\tilde{A}_p^* + i\Gamma_{cp}^{1/2}\tilde{S}_p, \end{aligned} \quad (1)$$

$$\begin{aligned} \frac{d\tilde{A}_s}{dt} &= [i(\Delta\omega_s + 2\gamma_{spsp} U_p + \gamma_{ssss} U_s) - \Gamma_{ts}/2] \tilde{A}_s \\ &\quad + i\gamma_{spip}\tilde{A}_p^2\tilde{A}_i^* + i\gamma_{spp}\tilde{A}_p^2 + i\Gamma_{cs}^{1/2}\tilde{S}_s, \end{aligned} \quad (2)$$

$$\begin{aligned} \frac{d\tilde{A}_i}{dt} &= [i(\Delta\omega_i + 2\gamma_{ipip} U_p + 2\gamma_{isis} U_s) - \Gamma_{ti}/2] \tilde{A}_i \\ &\quad + i\gamma_{ipsp}\tilde{A}_p^2\tilde{A}_s^*. \end{aligned} \quad (3)$$

The field amplitude is normalized so that $|\tilde{A}_{p,s,i}|^2 = U_{p,s,i}$ represents intracavity energy for pump (ω_p), signal and second-harmonic field ($\omega_s = 2\omega_p$), and idler dc field ($\omega_i = 0$), respectively. The first term in each equation describes the intracavity field evolution considering laser-cavity mode detuning ($\Delta\omega_{p,s,i}$), self- and cross-phase-modulation (SPM and XPM) from U_p and U_s , and cavity energy decay ($\Gamma_{tp,ts,ti}$). The second term in each equation describes the four-wave-mixing (FWM) interaction with ω_p (degenerate), ω_s , and ω_i . The third terms in the top two equations describe the second-harmonic interaction between pump and signal. The last terms in these two equations are the

source terms for pump and signal, where $P_{p,s}^{\text{in}} = |\tilde{S}_{p,s}|^2$ represents the input power in the waveguide, and $\Gamma_{cs,sp}$ is the waveguide-resonator coupling rate. In these equations, SPM, XPM, and FWM are all $\chi^{(3)}$ interactions described by the cavity nonlinear interaction γ_{mnuv} , where the subscripts $m, n, u, v = p, s, i$; and SHG is a $\chi^{(2)}$ interaction described by the cavity nonlinear interaction γ_{mnui} , where the subscripts $m, n, u = p, s$. Appendix B provides more details on the equations describing our system.

We first consider the ultrafast processes, including the cavity evolution, the SHG process, and the source terms, to get the initial state of the FWM process, which is much slower (due to CPG) and determines the threshold. When the cavity reaches equilibrium for these ultrafast processes, the intracavity optical energy is given by

$$U_p = \frac{\Gamma_{cp} P_p^{\text{in}}}{(\Delta\omega_p + \gamma_{pppp} U_p + 2\gamma_{psps} U_s)^2 + (\Gamma_{tp}/2)^2 + \gamma_{psp}^2 U_s^2}, \quad (4)$$

$$U_s = \frac{\Gamma_{cs} P_s^{\text{in}} + \gamma_{sp}^2 U_p^2}{(\Delta\omega_s + 2\gamma_{spsp} U_p + \gamma_{ssss} U_s)^2 + (\Gamma_{ts}/2)^2}, \quad (5)$$

with the assumption that pump power and energy dominates ($P_p^{\text{in}} \gg P_s^{\text{in}}$ and $U_p \gg U_s$), and $\chi^{(2)}$ OPO is not excited as the intrinsic $\chi^{(2)}$ nonlinearity is small. There are in general two solutions for these two quadratic equations, and we choose the one with larger intracavity pump power ($U_p > U_s$), as the other case ($U_p < U_s$) is irrelevant to our work.

We now consider the threshold of the slower FWM process. U_p needs to provide enough gain for the signal and idler to overcome their losses, and U_s has no effect on the threshold to the first order. In the case that cw lasers are used for pump and signal and the initial idler dc field is not present, the parametric threshold is given by

$$U_p = \frac{\Gamma_{cp} P_p^{\text{in}}}{(\Gamma_{tp}/2)^2 + \gamma_{psp}^2 \frac{\Gamma_{cs} P_s^{\text{in}}}{(\Gamma_{ts}/2)^2}} \geq \sqrt{\frac{(\Gamma_{ts}/2)(\Gamma_{ti}/2)}{\gamma_{spip} \gamma_{ipsp}}}, \quad (6)$$

where the detuning is assumed to be ideal, that is, zero relative cavity detuning after the Kerr (and thermal) shifts are considered, and U_p depends on P_p^{in} and P_s^{in} , together with the intrinsic second-order nonlinear interaction parameter (γ_{psp}).

In the single pump scheme ($P_s^{\text{in}} = 0$), considering that the intrinsic $\chi^{(2)}$ nonlinearity is small, to the first order, the threshold pump power is estimated by

$$U_p = \frac{\Gamma_{cp} P_p^{\text{in}}}{(\Gamma_{tp}/2)^2} \geq \sqrt{\frac{(\Gamma_{ts}/2)(\Gamma_{ti}/2)}{\gamma_{spip} \gamma_{ipsp}}}. \quad (7)$$

In particular, Γ_{ti} represents the decay rate of the idler (dc) intracavity energy. To estimate the timescale of this decay,

we consider the RC response of the material, so that $\Gamma_{ti} = 2/\tau$, where $\tau = \rho\epsilon_{dc}\epsilon_0$. Here τ is the decay time of the dc field, ρ is the electrical resistivity, ϵ_{dc} is the dc dielectric constant of the material, and ϵ_0 is the vacuum permittivity. This simple equation does not include the device microstructure, and hence is unlikely to provide a quantitatively accurate prediction. However, its simple functional form, based on parameters obtainable from the literature, provides a simple qualitative check of the characteristic decay time of the dc field inside a certain medium, e.g., from 0.27 to 15 s in Si_3N_4 and 9 h to 40 days in fused silica. These ranges of values are consistent with measurements from previous experiments within an order of magnitude [24,26]. Appendix C provides further details on related parameters, and Appendix D provides more discussion on τ of common photonics materials.

Importantly, the power threshold predicted by Eq. (7) is in close resemblance to a conventional $\chi^{(3)}$ OPO with the exception of one caveat—the definition of γ_{ipsp} . Following the traditional definition in nonlinear optics [30], we have

$$\gamma_{spip} = 3 \frac{\omega_s \eta_{spip} \chi_{spip}^{(3)}}{4\bar{n}_{spip}^4 \epsilon_0 \bar{V}_{spip}}, \quad (8)$$

$$\gamma_{ipsp} = 3 \frac{\omega_i \eta_{ipsp} \chi_{ipsp}^{(3)}}{4\bar{n}_{ipsp}^4 \epsilon_0 \bar{V}_{ipsp}}. \quad (9)$$

Here $\chi_{spip}^{(3)} = \chi_{ipsp}^{(3)}$ is guaranteed by quantum mechanics [18], and η_{mnuv} , \bar{n}_{mnuv} , and \bar{V}_{mnuv} are also identical for subscripts $mmuv = spip, ipsp$ (Appendix B). However, the dc field by definition has $\omega_i = 0$, which leads to $\gamma_{ipsp} = 0$, clearly in contradiction with the experiments, where the electric field can indeed be created (to the extent that strong effective $\chi^{(2)}$ effects are observed). An open question, however, is whether the generated field due to the CPG effect is necessarily a dc field ($\omega_i = 0$), or whether it can be at a nonzero frequency (still many orders of magnitude lower than the optical frequencies involved), which we hence refer to as a (quasi)-dc field. Ultimately, the true value of ω_i is related to the microscopic mechanism of the CPG process. However, Eq. (7) tells us that if the threshold behavior is observed in experiment, the threshold value gives us an estimate of γ_{ipsp} , which we can in turn use to better understand the nature of the (quasi)-dc field.

III. EXPERIMENTS ON dc KERR OPO

Our SHG device contains a Si_3N_4 microring integrated with two coupling waveguides, as shown in Fig. 2(a). Pump and signal waves are coupled by the top and bottom waveguides, respectively. As discussed previously,

three modes inside the microring are involved in the process, including an idler mode (i.e., dc electric mode), a pump mode (1558 nm), and a signal mode (779 nm). The dc mode has approximately zero frequency and momentum ($\omega \approx 0$ and $m = 0$). The pump mode is a fundamental transverse-electric (TE1) mode with $m = 154$ and the signal mode is a third-order transverse-electric (TE3) mode with $m = 308$, and transmission traces are shown in the insets of Figs. 2(b) and 2(c), respectively. The modes are identified by selective mode splitting [31] to guarantee the perfect phase matching. Figure 2(c) shows an example of the spectrum of the generated second-harmonic light, and we have confirmed in previous work [26] that SHG is the dominant process, with no Kerr comb generation of other four-wave-mixing processes present.

A threshold behavior is clearly observed when the laser is adiabatically tuned [Fig. 2(d)], where we show data both as a function of input wavelength (main figure) and dropped power in the cavity (inset). The threshold power is obtained from the latter, and its value of (2.3 ± 0.1) mW is on par with threshold levels we have recently observed for widely separated $\chi^{(3)}$ optical parametric oscillators in which all fields are in the optical domain [28]. This suggests that if our model is correct, the effective Q of the (quasi)-dc field should be of a similar order (approximately equal to 10^6), as we discuss further in the next section. For now, we note the qualitative agreement between the experiments and the model's prediction of a threshold for efficient SHG.

We also measure the temporal response of the SHG process [Fig. 2(e)], which provides additional confirmation of our theoretical model in several ways. First, when the pump is below threshold, e.g., the cyan curve (II) and blue (I1) curve in which the pump is at 1557.99 nm and 1557.98 nm, respectively, an initial large SHG and dc intracavity field cannot be sustained and therefore decays over time, in agreement with our prediction when below-threshold (but not fully explained through a typical effective $\chi^{(2)}$ theory). Second, the decay times agree with the RC time of Si_3N_4 (27 s), for which an estimate of the latter only involves the density and permittivity of Si_3N_4 . Above-threshold traces (yellow, orange, and red, labeled III, IV, and IV) grow faster than the RC time because of the above-threshold gain. Moreover, the three bottom subthreshold traces in blue (I1, I2, and I3) show that, at the same nominal laser-cavity detuning, the final steady-state signal level is identical regardless of the initial SHG levels. Finally, trace II taken just below threshold shows $\tau \approx 16$ s, which agrees with the RC time of Si_3N_4 . Thus, even without having a microscopic picture of the CPG effect, we are at least able to verify that the decay dynamics of the generated (quasi)-dc field are qualitatively in accordance with what one might expect based on the Si_3N_4 bulk parameters.

IV. UNCONVENTIONAL LIGHT AMPLIFICATION

A conventional OPA cannot turn into OPO without increasing the pump power above threshold, and the small-signal OPA gain is constant before the pump depletion starts to occur. In contrast, a careful revisit of Eq. (6) beyond the first-order approximation suggests that the weak intrinsic nonlinearity not only serves as the source of initial fields for dc Kerr OPO, but also predicts an unconventional light-amplification phenomenon, that is, a small input signal is not amplified with a certain small-signal gain (as in conventional OPA), but instead amplified to a fixed power level governed by the OPO condition. We verify this unconventional light amplification experimentally in Fig. 3.

To prepare the light amplification, we first tune the dc Kerr OPO process just below threshold, as shown in Fig. 3(a). When operating above threshold, the dc Kerr OPO takes about 30 s for the SHG output power to increase from 20 nW to 50 μ W. When we blueshift the pump in fine-tuning steps of 1 pm, we can maintain OPO below, but close, to threshold. After pump preparation, we increase the cw seed signal [Fig. 3(b)] for light amplification. The wavelength-dependent oscillation in power comes from an amplified spontaneous emission noise source, which is used as a cw seed. When the seed signal increases to -46 dBm at $\lambda \approx 779$ nm (dashed and solid green traces), the seed is amplified to -38 dBm in a few seconds (dashed green) and eventually to -19 dBm (solid green), which corresponds to a gain of nearly 27 dB. Unlike a traditional OPA, the signal power does not increase further as the cw seed level increases (the top three traces, in cyan, purple, and solid green), overlapping the same signal level of an OPO (the dashed red trace, in which no input field at the SHG frequency is sent into the cavity).

The SHG signal, without cw seed input, comes from the weak intrinsic $\chi^{(2)}$ nonlinearity, with a detected power approximately equal to -60 dBm, as shown in the inset of Fig. 3(b). The physical origin of this intrinsic nonlinearity remains to be examined, but can be from a surface-asymmetry effect [32]. Although we are working in an effective SHG regime, such light amplification can be extended to an effective sum-frequency generation (SFG) regime. We emphasize that dc $\chi^{(3)}$ SHG and SFG schemes allow light amplification at a higher frequency than the pump, which is forbidden in conventional $\chi^{(2)}$ OPO schemes.

The use of a broadband cw signal relieves the complication of Kerr shift and cavity detuning [Eq. (4)], so the unconventional light amplification is likely from the interplay of $\chi^{(2)}$ and dc Kerr OPO [Eq. (6)]. However, we note that it might be possible to observe such unconventional light amplification, more specifically, the reduction of OPO threshold power in near-threshold OPA, in a pure Kerr system (with a narrow-linewidth signal laser) under

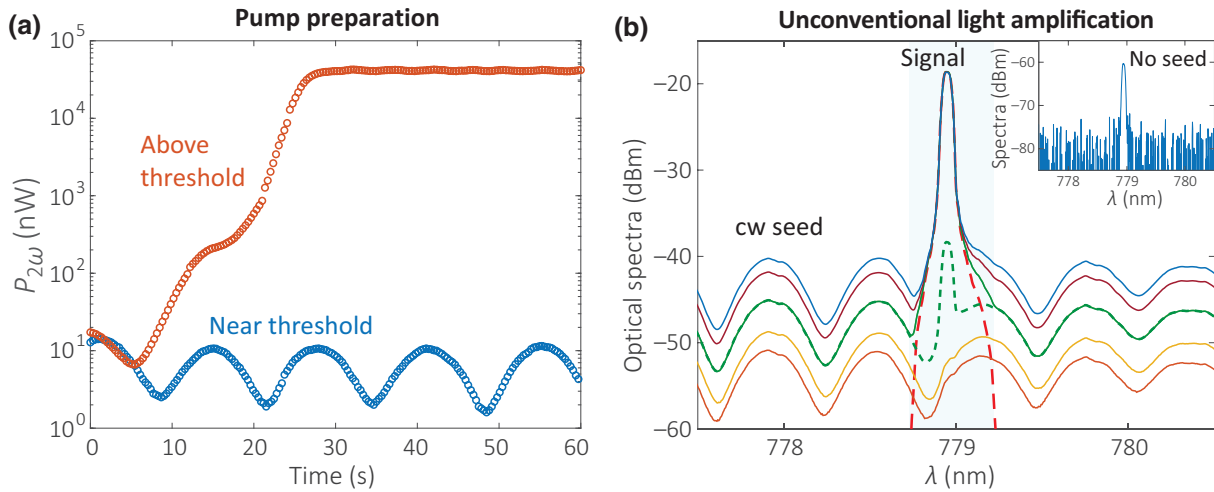


FIG. 3. Unconventional light amplification. (a) The system is prepared near (but below) the dc Kerr OPO threshold by fine control of pump detuning. (b) A cw input broadband seed signal is gradually increased from approximately equal to -53 dBm (red) to approximately equal to -43 dBm (blue) to activate light amplification of a narrowband signal around 779 nm. The spectral oscillation (8 to 10 dB) in the cw seed is from the amplified spontaneous emission source. The dashed and solid green traces (plotted within the light blue shaded region centered at 779 nm) represent the initial and final signal with the same cw seed. The peak signal, once the amplification is activated, is identical to the above-threshold case (approximately equal to -19 dBm, see the dashed red curve). This amplification regime is unique, and agrees with the theoretical prediction. The inset shows the optical spectrum without the cw seed, which is due to weak second-harmonic generation resulting from the small intrinsic SHG.

specific detuning and pump-probe power conditions. This effect has not been reported previously and requires further investigation (perhaps in a conventional close-band OPO).

V. REMARKS ON THE DC FIELD

The above experiments verify the existence of a threshold for efficient SHG and a decay time consistent with the silicon-nitride resistivity and dc permittivity. More quantitatively, we can examine what the value of the threshold power says about the (quasi)-dc field. In particular, substituting the threshold power, measured cavity decay rates for the optical fields, estimated decay rate for the (quasi)-dc field, and estimate for γ_{spip} in Eq. (7), we arrive at an estimate for γ_{ipsp} , which in turn [from Eq. (9)] gives us the estimate $\omega_i/2\pi \approx 10$ kHz. This suggests that the CPG effect in our system does not in fact generate a dc field, but instead has an ac frequency that, while 10 orders of magnitude smaller than the optical frequencies involved, is nevertheless nonzero. This frequency is similar to the linewidth of the external cavity diode laser we use as a 1550-nm pump source, and is approximately the maximum mismatch between pump and second harmonic allowed by frequency matching (energy conservation) [Fig. 2(c)].

This estimate for ω_i is equivalent to suggesting that the CPG process has a characteristic time of $\tau_c \approx 32$ μ s and an enhancement factor of $Q_{ii} = \tau/\tau_c = 4.5 \times 10^5$ —much larger than the previously reported value of 64 in a doped fiber [13]. Interestingly, this Q for the electric field is similar to typical Q s for the optical modes in a Si_3N_4 microring.

This similarity leads to the aforementioned similarity in the threshold powers of two processes—the current dc Kerr OPO process and the widely separated OPO involving three optical frequencies (four optical waves, with a degenerate pump) [28]. Further studies in our devices but with longer time constants [24] might help elucidate the microscopic nature of dc field.

VI. DISCUSSION

In summary, we propose the physical picture that recently observed photoinduced SHG in silicon-nitride microring resonators can be viewed as a four-wave-mixing optical parametric oscillation process that involves three optical fields (a degenerate pump and the second harmonic) and a quasi-dc field. This model is consistent with our experimental observation of a threshold for efficient SHG and unconventional light amplification that differs from the traditional $\chi^{(2)}/\chi^{(3)}$ OPA. Our observed threshold powers are consistent with a picture in which the quasi-dc field oscillates with a quality factor of 4.5×10^5 .

While our work is focused on a degenerate four-wave-mixing process in a microcavity, it can be applied to nondegenerate four-wave mixing and other geometries such as waveguides and fibers. In particular, in our framework waveguide and fiber-based photoinduced SHG is essentially a singly resonant dc Kerr OPO and OPA process, where the long-lasting dc field functions as a high- Q resonant mode (in contrast, we effectively have a triply resonant process in the microcavity). To this end, we give an

estimate of threshold powers in these systems in Appendix E, which is a theoretical estimate and is in agreement with the reported values within an order of magnitude. Our perspective of understanding photoinduced SHG as dc Kerr OPO provides an alternative vantage point through which such systems can be considered, while also presenting constraints on the (quasi)-dc field and its CPG model that require further investigation. In the future, the threshold power can be reduced to $10 \mu\text{W}$, if mode engineering and high Q_s s in this work can be combined with the long dc time constant [24] reported in a similar Si_3N_4 platform.

ACKNOWLEDGMENTS

The authors thank Jianqi Hu, Edgars Nitiss, and Camille-Sophie Brès for helpful discussions. This work is supported by the DARPA ACES and NIST-on-a-chip programs. X.L. acknowledges support under the Cooperative Research Agreement between the University of Maryland and NIST-PML, Award No. 70NANB10H193.

APPENDIX

In this Appendix, we provide more details regarding the history and background of photoinduced SHG, the equations used to describe photoinduced SHG, and its natural description as a dc Kerr optical parametric oscillation process, and the parameters used in the theoretical estimate of the threshold power. We then show a brief summary of field- and photoinduced SHG works, as well as the time constant of dc fields in common photonics materials. We also give an estimate of threshold powers in various optics and photonics systems. Finally, we present experimental data on unconventional light amplification in this system, which is in agreement with the theoretical predictions.

APPENDIX A: HISTORY AND BACKGROUND FOR PHOTOINDUCED SHG

Figure 1 in the main text gives a brief summary and timeline of research on photoinduced SHG, and here we provide additional details. To start, we note that FISH provides the basic perspective that the product of the $\chi^{(3)}$ nonlinearity and the applied dc electric field (E_{dc}) produces an effective second nonlinearity ($\chi_{\text{eff}}^{(2)}$) [17]. This elegant perspective has been widely used to explain the large SHG response in SiO_2 fiber [4–8,12], as SiO_2 has no intrinsic $\chi^{(2)}$ nonlinearity [30]. Surprisingly, the electric field required to provide a sufficiently large effective $\chi^{(2)}$ to explain the observed SHG efficiencies was found to be about 10^6 V/m to 10^7 V/m —close to the breakdown voltage of the medium [5,8]. Although the demonstration of FISH involved a spatially uniform dc field [17], the dc field can have a spatial profile to form a nonlinear grating for QPM [18,19], similar to that in periodically poled crystals [33]. For example, FISH and QPM have been combined

in a periodically dc gated silicon waveguide to produce 13 %/W SHG efficiency [34].

In doped fibers, the nonlinear grating combining FISH and QPM can be formed optically with self-organized periods [4–8,12,16], through the CPG driven by the injected laser field at the fundamental frequency and a second optical field, at the second-harmonic frequency, which can be either from any seedling $\chi^{(2)}$ nonlinearity in the medium (e.g., due to symmetry breaking) [1,2] or through a separate laser [4,7]. A multiphoton CPG theory was proposed later on, in which two characteristic times are used (one describing the CPG interaction time, and the other describing the decay time of the field) [13]. It was also found that an ultraviolet laser can be used to erase the grating [9], and that the induced signal has a $\pi/2$ phase lag [15]. In recent years, there has been a revival of interest in studying photoinduced SHG in Si_3N_4 waveguides [20–22,24,25]. The operating power in these waveguides is reduced to 10 W [20], which is an over 100 times reduction compared to earlier fiber works. The generated nonlinear grating, whose periods can be self-organized in a manner similar to the doped fibers, can be visualized in real time by second-harmonic-generation microscopy [23], and can last over 20 days at room temperature [24].

Besides the original scheme that used a single pump laser [1,2], three other schemes were developed for this nonlinear grating, all using two fields, including one pump field and another second harmonic or dc field. First, a pump laser and its second-harmonic laser can write the grating together, and the grating can later be used for SHG [4]. Second, a pump laser and a relative weak second-harmonic seedling laser can initiate the grating, resulting in strong SHG output at the end [7]. Third, a pump laser and externally provided dc voltage can also write the grating [8]. All pump powers reported are high, ranging from 1 to 5 kW [2,4,6,7,10,12]. In part driven by the observations of various coherent excitation schemes [1,4,7,8], CPG was studied theoretically [11] and proposed to explain the large electric field in doped fibers [12]. Since then, FISH, QPM, and CPG formed the backbone of the understanding of photoinduced SHG [3].

APPENDIX B: A DESCRIPTION OF PHOTOINDUCED SHG INCLUDING $\chi^{(2)}$ AND $\chi^{(3)}$

In this section, we give more details on the equations we provide in the main text, starting with the following:

$$\frac{d\tilde{A}_p}{dt} = [i(\Delta\omega_p + \gamma_{pppp}U_p + 2\gamma_{psps}U_s) - \Gamma_{tp}/2]\tilde{A}_p + 2i\gamma_{pspi}\tilde{A}_s\tilde{A}_i\tilde{A}_p^* + i\gamma_{psp}\tilde{A}_s\tilde{A}_p^* + i\Gamma_{cp}^{1/2}\tilde{S}_p, \quad (\text{B1})$$

$$\begin{aligned} \frac{d\tilde{A}_s}{dt} &= [i(\Delta\omega_s + 2\gamma_{spsp} U_p + \gamma_{ssss} U_s) - \Gamma_{ts}/2] \tilde{A}_s \\ &\quad + i\gamma_{spip}\tilde{A}_p^2\tilde{A}_i^* + i\gamma_{spp}\tilde{A}_p^2 + i\Gamma_{cs}^{1/2}\tilde{S}_s, \end{aligned} \quad (\text{B2})$$

$$\begin{aligned} \frac{d\tilde{A}_i}{dt} &= [i(\Delta\omega_i + 2\gamma_{ipip} U_p + 2\gamma_{isis} U_s) - \Gamma_{ti}/2] \tilde{A}_i \\ &\quad + i\gamma_{ipsp}\tilde{A}_p^2\tilde{A}_i^*. \end{aligned} \quad (\text{B3})$$

As mentioned in the main text, these equations already assume perfect phase matching, that is, $m_s = 2m_p$ and $m_i = 0$. The field amplitude is normalized so that $U_m = |\tilde{A}_m|^2$ where $m = \{p, s, i\}$ represents intracavity energy for pump, signal, and idler, respectively. Here for pump and signal modes, $U_m = |\tilde{A}_m|^2 \approx \int_V dv \epsilon_m |\tilde{E}_m|^2$, as both electrical and magnetic energies are considered, represented by the dominant electric field only. This approximation is made possible when the other electric field components are much smaller than the dominant one, for example, $|\tilde{E}_z|$, $|\tilde{E}_\phi| \ll |\tilde{E}_r|$ for transverse-electric-like (TE) modes. For the idler field, the energy comes from the static electric field only, $U_i = |\tilde{A}_i|^2 = \int_V dv (1/2)\epsilon_i |\tilde{E}_i|^2$.

The first terms describe the cavity evolution considering Kerr shifts. The cavity detuning without Kerr shifts is $\Delta\omega_m = \omega_m - \omega_{m0}$, where ω_{m0} represents the center of the Lorentzian resonances for pump and signal and $\omega_{i0} = 0$ for the idler mode. The self- and cross-phase-modulation (SPM and XPM) redshift and decrease cavity resonance frequencies, depending on intracavity optical energies (U_p , U_s) and cavity nonlinear parameters, which is introduced later with four-wave-mixing interactions in Eq. (B5). Γ_{lm} describes the decay of the intracavity energy U_m , which includes the intrinsic cavity loss and the out coupling to waveguide, $\Gamma_{lm} = \Gamma_{0m} + \Gamma_{cm}$. Here the decay term Γ_{lm} is related to optical quality factor Q_{lm} or the field coupling and decay time τ_{lm} by

$$\Gamma_{lm} = \frac{\omega_{0m}}{Q_{lm}} = \frac{2}{\tau_{lm}}, \quad (l = t, 0, c; m = p, s, i). \quad (\text{B4})$$

For the idler mode, in particular, the decay time can be estimated by the RC time of the material, $\tau_{ti} = \rho n^2 \epsilon_0$.

The second terms describe the four-wave-mixing interaction with degenerate pump, signal, and idler. Both Kerr shifts and four-wave mixing interaction are $\chi^{(3)}$ processes, and the involved nonlinear interaction γ_{mnuv} is given by

$$\gamma_{mnuv} = \frac{3\omega_m \eta_{mnuv} \chi_{mnuv}^{(3)}}{4\bar{n}_{mnuv}^4 \epsilon_0 \bar{V}_{mnuv}}, \quad (\text{with } m, n, u, v = p, s, i), \quad (\text{B5})$$

which is a positive real parameter. $\chi_{mnuv}^{(3)}$ is abbreviation for $\chi^{(3)}(-\omega_m; \omega_n, -\omega_u, \omega_v)$, which describe the generation of ω_m and ω_u fields with the annihilation of ω_n and ω_v fields. η_{mnuv} characterizes the spatial overlap of such $\chi_{mnuv}^{(3)}$

interaction,

$$\eta_{mnuv} = \frac{\int_V dv \sqrt{\epsilon_m \epsilon_n \epsilon_u \epsilon_v} \tilde{E}_m^* \tilde{E}_n \tilde{E}_u^* \tilde{E}_v}{\prod_{j=m,n,u,v} (\int_V dv \epsilon_j^2 |\tilde{E}_j|^4)^{1/4}}, \quad (\text{B6})$$

which is dimensionless. \bar{n}_{mnuv} represents average linear refractive index $\bar{n}_{mnuv} = (n_m n_n n_u n_v)^{1/4}$. Likewise, \bar{V}_{mnuv} represents an average mode volume $\bar{V}_{mnuv} = (V_m^{(3)} V_n^{(3)} V_u^{(3)} V_v^{(3)})^{1/4}$, where the individual mode volume for a $\chi^{(3)}$ interaction is given by

$$V_m^{(3)} = \frac{(\int_V dv \epsilon_m |\tilde{E}_m|^2)^2}{\int_V dv \epsilon_m^2 |\tilde{E}_m|^4}, \quad (\text{with } m = p, s, i). \quad (\text{B7})$$

The third terms in Eq. (B1)–(B2) represent the second-harmonic-generation interaction, a $\chi^{(2)}$ process, where its cavity nonlinear parameter is given by

$$\gamma_{mnu} = \frac{3\omega_m \eta_{mnu} \chi_{mnu}^{(2)}}{4\sqrt{2}\bar{n}_{mnu}^3 \sqrt{\epsilon_0} \bar{V}_{mnu}}, \quad (\text{with } m, n, u = p, s), \quad (\text{B8})$$

which is a real parameter. η_{mnu} characterizes the spatial overlap of interacting optical modes, and is invariant regarding to the permutation of indices,

$$\eta_{psp} = \eta_{spp} = \frac{\int_V dv \epsilon_p \tilde{E}_p^2 \sqrt{\epsilon_s} \tilde{E}_s^*}{\prod_{j=p,p,s} (\int_V dv |\sqrt{\epsilon_j} \tilde{E}_j|^3)^{1/3}}, \quad (\text{B9})$$

which is dimensionless. $\chi^{(2)}$ is short for $\chi^{(2)}(\omega_p; \omega_s, \omega_p)$ and $\chi^{(2)}(\omega_s; \omega_p, \omega_p)$, which are equal in a lossless medium. The averaged index here is given by $\bar{n} = (n_p^2 n_s)^{1/3}$. Similarly, the mode volume is given by \bar{V}_{mnu} and represents average mode volume that is invariant under permutation $\bar{V}_{psp} = \bar{V}_{spp} = [(V_p^{(2)})^2 V_s^{(2)}]^{1/3}$, where $V_{p,s}^{(2)}$ is given by

$$V_m^{(2)} = \frac{(\int_V dv \epsilon_m |\tilde{E}_m|^2)^3}{(\int_V dv |\sqrt{\epsilon_m} \tilde{E}_m|^3)^2}, \quad (\text{with } m = p, s). \quad (\text{B10})$$

The fourth terms in the top two equations describe the second-harmonic interaction between pump and signal. The last terms in these two equations are the source terms for pump and signal, where $P_{p,s}^{\text{in}} = |\tilde{S}_{p,s}|^2$ represents the input power in the waveguide.

APPENDIX C: PARAMETERS USED TO ESTIMATE THE POWER THRESHOLD

In the main text, we give a lower-bound estimate for the threshold power of photoinduced SHG; here, we provide a detailed list of values for the related parameters. The

TABLE I. Parameters in use to estimate the threshold of photoinduced SHG.

| $\omega_p/(2\pi)$ | Q_{ep} | Q_{tp} | Q_{ts} | Q_{ti} | \bar{n}_{ipsp} | \bar{V}_{ipsp} | η_{ipsp} | $\chi_{ipsp}^{(3)}$ |
|-------------------|-------------------|-------------------|-------------------|-------------------|------------------|----------------------|---------------|---|
| 192.55 THz | 6.0×10^5 | 1.2×10^6 | 1.6×10^6 | 8.6×10^5 | 2.0 | $62.2 \mu\text{m}^3$ | 0.573 | $3.39 \times 10^{-21} \text{ m}^2/\text{V}^2$ |

equation describing the threshold power is given by Eq. (7) in the main text,

$$P_p^{\text{in}} \geq \frac{\Gamma_{tp}^2}{8\Gamma_{cp}} \sqrt{\frac{\Gamma_{ts}\Gamma_{ti}}{\gamma_{spip}\gamma_{ipsp}}} \quad (\text{C1})$$

Substituting Eqs. (B4)–(B5) into this equation, we have

$$P_p^{\text{in}} \geq \frac{\omega_p Q_{ep}}{Q_{tp}^2 \sqrt{Q_{ts} Q_{ti}}} \frac{\epsilon_0 \bar{n}_{ipsp}^4 \bar{V}_{ipsp}}{6 \eta_{ipsp} \chi_{ipsp}^{(3)}} \quad (\text{C2})$$

The parameters are given in Table I, where the dc field is assumed to be uniformly distributed inside the ring. A realistic model considering the radial profile of the dc mode is likely to lead to a smaller effective volume and a larger mode overlap, and therefore a smaller estimate of threshold power. The $\chi_{ipsp}^{(3)}$ is calculated from n_2 in Ref. [35] following $\chi^{(3)} = (4/3)n^2\epsilon_0 cn_2$, where n is the refractive index, ϵ_0 is the vacuum permittivity constant, and c is the speed of light [30].

APPENDIX D: A TABLE COMPARING TIME CONSTANTS OF COMMON PHOTONICS MATERIALS

In Table II, we show the estimate of time constants of common photonics materials. We note that the long duration time in fused silica has been widely reported

TABLE II. Comparison of time constants of common photonic materials via the RC model. The electrical resistivity (ρ) is a key parameter for the time constant, as ϵ_{dc} are typically within one order of magnitude for different materials. We note that the specific values of ρ can vary significantly because of the growth method and material purity, and for this reason the time constants derived in this table are for general guidance only.

| Material | ϵ_{dc} | $\rho (\Omega \text{ m})$ | Time constant |
|-------------------------|-----------------|---|---------------|
| Fused silica | 3.6–3.9 | $1 \times 10^{15} - 1 \times 10^{17}$ | 9 h–40 days |
| Al_2O_3 | 7.8–11.1 | $1 \times 10^{10} - 1 \times 10^{16}$ | 1 s–11 days |
| LiNbO_3 | 28 | $2.4 \times 10^9 - 3.8 \times 10^{12}$ | 0.6 s–16 min |
| AlN | 8.3–9.3 | $1 \times 10^9 - 1 \times 10^{13}$ | 0.07 s–14 min |
| Si_3N_4 | 9.5 | $3.16 \times 10^9 - 1.73 \times 10^{11}$ [36] | 0.27 s–15 s |

ρ values for fused silica, Al_2O_3 , and AlN are from AZO materials [42]; and ρ for LiNbO_3 is from Roditi International Corporation [37].

[1,2,4,6,7], and that the long duration time reported in a Si_3N_4 waveguide [24] may be due to the surrounding oxide rather than the Si_3N_4 core. In particular, Si_3N_4 waveguides without a top and side SiO_2 cladding have reported shorter times [23] on par with our observations in Si_3N_4 ring resonators without a top and side SiO_2 cladding.

APPENDIX E: AN ESTIMATE OF THRESHOLD POWERS IN DIFFERENT SYSTEMS

Here, we give a rough estimate of the threshold powers for dc Kerr OPO in different systems (Table III), based on Eq. (C2) above and a comparison of the relevant parameters in these systems against their values in our microring resonators. First, we note that without cavity enhancement, but in a nanophotonic waveguide with perfect phase matching, the power threshold is expected to increase as both pump and signal are propagating waves without resonant enhancement. We can estimate the threshold by considering the scaling of the threshold with finesse. As our microring resonator has a finesse $\mathcal{F} \approx 5000$ (compared to a waveguide finesse $\mathcal{F} = 1$) and time constant of 15 s (compared to a time constant of 21 days [24]), the overall factor of increase in the threshold power is $5000^{1.5}/(21 \times 24 \times 3600/15)^{0.5} \approx 1000$, resulting in an expected threshold power of approximately equal to 2 W.

Next, we consider the case of an optical fiber (which does not have nanophotonic confinement). Its area is approximately $80 \mu\text{m}^2$ (assuming 10- μm mode-field diameter), which is $200\times$ larger than the $0.4 \mu\text{m}^2$ mode area of a Si_3N_4 nanophotonic waveguide. Considering also the difference in refractive index that contributes to a scaling factor of $(1.5/2.0)^4$ to the threshold, and $\chi^{(3)}$ nonlinearity that contributes a scaling factor of $(3.39 \times 10^{-21}/2.5 \times 10^{-22})$ to the threshold, the power threshold is approximately $850 \times$ of the nanophotonic waveguide case, that is, approximately 2 kW.

These estimates align with the reported values from experiments in nanophotonic waveguides [24] and silica fibers [12] to within an order of magnitude. A more accurate estimate requires the consideration of the exact parameters as well as the details of the quasi-phase-matching and pulse-pumping schemes. We note that such a theoretical estimate (at any level of accuracy) has not so far been reported. We believe that such estimates should be possible now, using the conceptual framework for photoinduced SHG that we introduce in this work.

TABLE III. Comparison of photoinduced SHG including schemes, peak conversion efficiencies, threshold powers, duration, and relevant models and theories. High optical pump powers are needed in single-pump photoinduced SHG in general; in resonators, large circulating intensities are created at lower powers through cavity enhancement. The listed threshold powers are the upper-bound values in the corresponding systems. Outside of the current work, only in two cases (in bold) have threshold powers been explicitly reported [2,20]. The top part of the table includes experimental works (some of which contain supporting theory), while the bottom part includes works that are primarily theoretical.

| Year | Laser | Platform | $\eta = P_{2\omega}/P_\omega$ | P_{th} | Time | Model, scheme, or theory ^R | Summary |
|-------------|--------------|---------------------------------|-------------------------------|---|------------------|--|--|
| 1962 | Pulse | Bulk [17] | — | No threshold | — | $\chi^{(2)} \sim \chi^{(3)} E_{\text{dc}}$ (implied) | $\chi_{\text{eff}}^{(2)}$ (1st) descriptive |
| 1986 | Pulse | Fiber [1] | $\sim 3\%$ | Not reported | h | Weak SHG initiation before exponential growth | empirical |
| 1987 | Pulse | Fiber [2] | > 5 % | 5 kW^P | h | $\mathbf{P}_{2\omega}(\mathbf{nW}) = 0.54\exp(3.1\mathbf{gt})$ with $\mathbf{g} = 8.6\mathbf{P}(\mathbf{W}) - 0.6^A$ | $\chi_{\text{eff}}^{(2)}$ |
| 1987 | Pulse | Fiber [4] | 0.1 % | Dual-pump writing | h | $P_{2\omega}/P_{2\omega}^0 = 4(P_\omega/P_\omega^0)^2 \sin^2(\alpha L/2)$, α not given | $\chi_{\text{eff}}^{(2)}$ |
| 1987 | Pulse | Fiber [6] | 0.5 % | < 10 kW ^P | h | Spatial grating of dipole color centers | $\chi_{\text{eff}}^{(2)}$ |
| 1988 | Pulse | Fiber [7] | 0.24 % | Pump + seedling | h | $P_{2\omega}/P_{2\omega}^0 = \text{sinc}^2(\Delta k L/2)$ | $\chi_{\text{eff}}^{(2)}$ |
| 1988 | Pulse | Fiber [8] | 0.001 % | Laser + dc writing | — | High voltage with laser pump to write grating | $\chi_{\text{eff}}^{(2)}$ |
| 1989 | Pulse | Fiber [12] | 0.003 % | < 1 kW ^P +300 W ^P | 1 h | Coherent photogalvanic mechanism | descriptive; $\chi_{\text{eff}}^{(2)}$ |
| 1989 | — | — | — | < 3 kW ^P +120 W ^P | — | $\pi/2$ phase observed; questions on self-organized SHG [10] | — |
| 1991 | — | — | — | — | — | $\chi^{(2)}(t) \sim P_{2\omega}^{1.5} P_\omega^1$ initially; interference of ionization [38] | — |
| 1993 | — | — | — | — | — | $\pi/2$ phase confirmed in bulk crystal [15] | — |
| 2017 | Pulse | wg [20] | 0.4 % | 10 W^P | Min | $\mathbf{R}(1\mathbf{s}) = (\mathbf{P}-\mathbf{P}_{\text{th}})/\mathbf{F}$ with \mathbf{P}_{th} and \mathbf{F} fitted | Empirical; $\chi_{\text{eff}}^{(2)}$ |
| 2017 | cw | wg [21] | 0.05 %/W | < 60 W ^P | Min | Grating poled by pulse | $\chi_{\text{eff}}^{(2)}$ |
| 2019 | Pulse | wg [23] | 0.005 %/W | — | A few 10 s | Grating poled by pulse | $\chi_{\text{eff}}^{(2)}$ |
| 2019 | cw | wg [22] | 0.08 %/W | — | — | Grating poled by pulse | $\chi_{\text{eff}}^{(2)}$ |
| 2019 | cw | wg [24] | 0.31 %/W | < 38 W ^P | 20 days | Grating poled by pulse, lasting 20 days | $\chi_{\text{eff}}^{(2)}$ |
| 2020 | Pulse | wg [25] | 0.5 %/W | — | Min | Grating poled by pulse | $\chi_{\text{eff}}^{(2)}$ |
| 2020 | cw | Ring [26] | 2,500 %/W | < 4 mW | < 1 ~ 110 s | High-Q cavity and perfect phase matching | $\chi_{\text{eff}}^{(2)}$ |
| 2021 | cw | Ring [27] | 51 %/W | < 500 mW | 20 days | High-Q cavity and automatic quasi-phase-matching | Eq. (C.2) |
| 2021 | cw | Ring^{This work} | 500 %/W | 2.3 mW | 10 ~ 30 s | dc Kerr optical parametric oscillation | $\chi_{\text{eff}}^{(2)}$ |
| 1987 | Pulse | Fiber [5] | — | — | — | Comprehensive discussion with $E_{\text{dc}} = 10^7 \text{ V/m}$ | — |
| 1988 | Pulse | Fiber [9] | — | — | — | Erasing grating with UV; macroscopic explanation | — |
| 1988 | Pulse | Fiber [39,40] | — | — | — | Challenging existing effective $\chi^{(2)}$ theory | — |
| 1989 | — | — | — | — | — | Coherent photogalvanic effect [11] | — |
| 1990 | Pulse | Fiber [41] | — | — | — | Support current effective $\chi^{(2)}$ theory | — |
| 1991 | Pulse | Fiber | — | — | — | Asymmetric $< E^3 >$ photoionization [14] | — |
| 1991 | Pulse | — | — | — | — | High-order ionization and two characteristic times [13] | — |

^R Only models, schemes, and theories related to the threshold behavior are listed in the table. Please refer to the references for more details. ^P Peak powers are listed when pulsed lasers are used, as it is the relevant parameter for nonlinear optics. ^A This empirical equation from Ref. [2] is written in terms of average power instead of peak power. wg: waveguides.

- [1] U. Österberg and W. Margulis, Dye laser pumped by Nd:YAG laser pulses frequency doubled in a glass optical fiber, *Opt. Lett.* **11**, 516 (1986).
- [2] U. Österberg and W. Margulis, Experimental studies on efficient frequency doubling in glass optical fibers, *Opt. Lett.* **12**, 57 (1987).
- [3] E. M. Dianov and D. S. Starodubov, Photoinduced generation of the second harmonic in centrosymmetric media, *Quant. Electron.* **25**, 395 (1995).
- [4] R. H. Stolen and H. W. K. Tom, Self-organized phase-matched harmonic generation in optical fibers, *Opt. Lett.* **12**, 585 (1987).
- [5] R. W. Terhune and D. A. Weinberger, Second-harmonic generation in fibers, *J. Opt. Soc. Am. B* **4**, 661 (1987).
- [6] M. C. Farries, P. S. J. Russell, M. E. Fermann, and D. N. Payne, Second-harmonic generation in an optical fibre by self-written $\chi^{(2)}$ grating, *Electron. Lett.* **25**, 395 (1987).
- [7] H. W. K. Tom, R. H. Stolen, G. D. Aumiller, and W. Pleibel, Preparation of long-coherence-length second-harmonic-generating optical fibers by using mode-locked pulses, *Opt. Lett.* **13**, 512 (1988).
- [8] M.-V. Bergot, M. C. Farries, M. E. Fermann, L. Li, L. J. Poynitz-Wright, P. S. J. Russell, and A. Smithson, Generation of permanent optically induced second-order nonlinearities in optical fibers by poling, *Opt. Lett.* **13**, 592 (1988).
- [9] F. Ouellette, K. O. Hill, and D. C. Johnson, Light-induced erasure of self-organized $\chi^{(2)}$ gratings in optical fibers, *Opt. Lett.* **13**, 515 (1988).
- [10] W. Margulis, I. C. S. Carvalho, and J. P. von der Weid, Phase measurement in frequency-doubling fibers, *Opt. Lett.* **14**, 700 (1989).
- [11] M. V. Éntin, Theory of the coherent photovoltaic effect, *Sov. Phys. Semicond.* **23**, 664 (1989).
- [12] E. M. Dianov, P. G. Kazanskii, and D. Y. Stepanov, Problem of the photoinduced second harmonic generation in optical fibers, *Sov. J. Quant. Electron.* **19**, 575 (1989).
- [13] D. Z. Anderson, V. Mizrahi, J. E. Sipe, and C. Ban, Model for second-harmonic generation in glass optical fibers based on asymmetric photoelectron emission from defect sites, *Opt. Lett.* **16**, 796 (1991).
- [14] B. Baranova, A. N. Chudinov, and A. A. Shul, Theory and observation of polar asymmetry of photoionization in a field with $\langle E^3 \rangle \neq 0$, *Zh. Eksp. Teor. Fiz.* **98**, 1857 (1990).
- [15] M. A. Bolshtyansky, V. M. Churikov, Y. E. Kapitzky, A. Y. Savchenko, and B. Y. Zel'dovich, Phase properties of $\chi^{(2)}$ gratings in glass, *Opt. Lett.* **18**, 1217 (1993).
- [16] W. Margulis, F. Laurell, and B. Lesche, Imaging the nonlinear grating in frequency-doubling fibres, *Nature* **378**, 699 (1995).
- [17] R. W. Terhune, P. D. Maker, and C. M. Savage, Optical Harmonic Generation in Calcite, *Phys. Rev. Lett.* **8**, 404 (1962).
- [18] J. A. Armstrong, N. Bloembergen, J. Ducuing, and P. S. Pershan, Interactions between light waves in a nonlinear dielectric, *Phys. Rev.* **127**, 1918 (1962).
- [19] P. A. Franken and J. F. Ward, Optical harmonics and nonlinear phenomena, *Rev. Mod. Phys.* **35**, 23 (1963).
- [20] M. A. Porcel, J. Mak, C. Taballione, V. K. Schermerhorn, J. P. Epping, P. J. van der Slot, and K.-J. Boller, Photoinduced second-order nonlinearity in stoichiometric silicon nitride waveguides, *Opt. Express* **25**, 33143 (2017).
- [21] A. Billat, D. Grassani, M. H. P. Pfeiffer, S. Kharitonov, T. J. Kippenberg, and C.-S. Brès, Large second harmonic generation enhancement in Si_3N_4 waveguides by all-optically induced quasi-phase-matching, *Nat. Commun.* **8**, 1016 (2017).
- [22] D. Grassani, M. H. P. Pfeiffer, T. J. Kippenberg, and C.-S. Brès, Second- and third-order nonlinear wavelength conversion in an all-optically poled Si_3N_4 waveguide, *Opt. Lett.* **44**, 106 (2019).
- [23] D. D. Hickstein, D. R. Carlson, H. Mundoor, J. B. Khurgin, K. Srinivasan, D. Westly, A. Kowlgy, I. I. Smalyukh, S. A. Diddams, and S. B. Papp, Self-organized nonlinear gratings for ultrafast nanophotonics, *Nat. Photon.* **13**, 494 (2019).
- [24] E. Nitiss, T. Liu, D. Grassani, M. Pfeiffer, T. J. Kippenberg, and C.-S. Brès, Formation rules and dynamics of photoinduced $\chi^{(2)}$ gratings in silicon nitride waveguides, *ACS Photon.* **7**, 147 (2020).
- [25] E. Nitiss, O. Yakar, A. Stroganov, and C.-S. Brès, Highly tunable second-harmonic generation in all-optically poled silicon nitride waveguides, *Opt. Lett.* **45**, 1958 (2020).
- [26] X. Lu, G. Moille, A. Rao, D. A. Westly, and K. Srinivasan, Efficient photo-induced second harmonic generation in silicon nitride photonics, *Nat. Photon.* **15**, 131 (2021).
- [27] E. Nitiss, J. Hu, A. Stroganov, and C.-S. Brès, Optically reconfigurable quasi-phase-matching in silicon nitride microresonators, *arXiv:2103.10222v1* (2021).
- [28] X. Lu, G. Moille, A. Singh, Q. Li, D. A. Westly, A. Rao, S.-P. Yu, T. C. Briles, S. B. Papp, and K. Srinivasan, Milliwatt-threshold visible-telecom optical parametric oscillation using silicon nanophotonics, *Optica* **6**, 1535 (2019).
- [29] X. Guo, C.-L. Zou, and H. X. Tang, Second-harmonic generation in aluminum nitride microrings with 2500 %/W conversion efficiency, *Optica* **3**, 1126 (2016).
- [30] R. W. Boyd, *Nonlinear Optics* (Academic Press, Amsterdam, 2008).
- [31] X. Lu, S. Rogers, W. C. Jiang, and Q. Lin, Selective engineering of cavity resonance for frequency matching in optical parametric processes, *Appl. Phys. Lett.* **105**, 151104 (2014).
- [32] X. Zhang, Q.-T. Cao, Z. Wang, Y.-X. Liu, C.-W. Qiu, L. Yang, Q. Gong, and Y.-F. Xiao, Symmetry-breaking-induced nonlinear optics at a microcavity surface, *Nat. Photon.* **13**, 21 (2019).
- [33] D. Feng, N. B. Ming, J. F. Hong, Y. S. Yang, J. S. Zhu, Z. Yang, and Y. N. Wang, Enhancement of second-harmonic generation in LiNbO_3 crystals with periodic laminar ferroelectric domains, *Appl. Phys. Lett.* **37**, 607 (1980).
- [34] E. Timurdogan, C. V. Poulton, M. J. Byrd, and M. R. Watts, Electric field-induced second-order nonlinear optical effects in silicon waveguides, *Nat. Photon.* **11**, 200 (2017).
- [35] K. Ikeda, R. E. Saperstein, N. Alic, and Y. Fainman, Thermal and Kerr nonlinear properties of plasma-deposited silicon nitride/silicon dioxide waveguides, *Opt. Express* **16**, 12987 (2008).

- [36] O. A. Lukianova, A. N. Khmara, S. N. Perevislov, D. A. Kolesnikov, and V. V. Krasilnikov, Electrical resistivity of silicon nitride produced by various methods, *Ceram. Int.* **45**, 9497 (2019).
- [37] The identification of any commercial website or company name is used to foster understanding. Such identification does not imply recommendation or endorsement or by the National Institute of Standards and Technology, nor does it imply that the materials or equipment identified are necessarily the best available for the purpose, <http://www.roditi.com/SingleCrystal/LiNbO3/liNBO3-Properties.html>.
- [38] A. Kamal, R. W. Terhune, and D. A. Weinberger, in *International Workshop on Photoinduced Self-Organization* *Effects in Optical Fiber* edited by F. Ouellette International Society for Optics and Photonics (SPIE, Quebec City, 1991), vol. 1516, p. 137.
- [39] V. Mizrahi, U. Österberg, J. E. Sipe, and G. I. Stegeman, Test of a model of efficient second-harmonic generation in glass optical fibers, *Opt. Lett.* **13**, 279 (1988).
- [40] V. Mizrahi, U. Österberg, C. Krautschik, G. I. Stegeman, J. E. Sipe, and T. F. Morse, Direct test of a model of efficient second-harmonic generation in glass optical fibers, *Appl. Phys. Lett.* **53**, 557 (1988).
- [41] V. Mizrahi, Y. Hibino, and G. Stegeman, Polarization study of photoinduced second-harmonic generation in glass optical fibers, *Opt. Commun.* **78**, 283 (1990).
- [42] <https://www.azom.com>